DOI: **10.37943/25IQAH4178**

Yeldos Zhandaulet
Master's degree, Senior Lecturer, School of Artificial Intelligence and Data Science
yeldos.zhandaulet@astanait.edu.kz, orcid.org/0000-0003-2954-8769
Astana IT University, Kazakhstan
Daulet Abilkairov
MBA, Head of the Project Management Unit
pmu_field@qazsu.kz, orcid.org/0000-0003-0850-7490
KazWater-IsDB, Kazakhstan
Alexandr Neftissov
PhD, Associate Professor, Rectorate for Science and Innovation
alexandr.neftissov@astanait.edu.kz, orcid.org/0000-0003-4079-2025
Academy of Physical Education and Mass Sports, Kazakhstan
PhD, Associate Professor, Researcher, Scientific-Innovation Center Industry 4.0
Astana IT University, Kazakhstan
Ilyas Kazambayev
Master's degree, Acting Director of Scientific-Innovation Center Industry 4.0
i.kazambayev@astanait.edu.kz, orcid.org/0000-0003-0850-7490
Astana IT University, Kazakhstan
Marat Bayandin
Doctor of Economics, Associate Professor, Department of Economics and Management
b1971ma@gmail.com, orcid.org/0000-0002-2158-4370
International Taraz University named after Sherkhan Murtaza, Taraz
Lalita Kirichenko
PhD student, Junior Researcher of Scientific-Innovation Center Industry 4.0
l.kirichenko@astanait.edu.kz, orcid.org/0000-0001-7069-5395
Astana IT University, Kazakhstan

NUMERICAL STUDY OF THE WATER SURFACE MOVEMENT DURING A DAM BREAK ON A REAL TERRAIN OF THE TASOTKEL RESERVOIR, ZHAMBYL REGION, KAZAKHSTAN

Abstract: This work presents a comprehensive numerical simulation of the dam-break process at the Tasotkel reservoir, located in real terrain conditions in the Zhambyl region. The study focuses on understanding how the released water mass propagates over complex topography and how terrain irregularities influence wave dynamics and inundation patterns. A Volume of Fluid method was employed to model the free-surface evolution of dam-break flows and their subsequent impact on flooding within the downstream valley. This approach allows accurate tracking of interface deformation and the movement of water over uneven ground. To validate the numerical model and ensure the reliability of the applied methodology, a set of controlled dam break simulations was carried out. These include dam-break tests in a channel with a trapezoidal recess and scenarios in an inclined channel. The outcomes of these simulations were compared against known reference data, demonstrating strong agreement and confirming the capability and accuracy of the proposed computational approach. The results reveal that the developed numerical model captures key flow features, such as wave arrival time, flow depths, and velocity variations over different terrain structures. The outcomes confirm that the method can be effectively used for high-precision and efficient assessment of dam-break consequences, including inundation zones and possible risks to downstream infrastructure or settlements. The main objective of this study is to provide a robust numerical framework for analyzing floods and inundation processes caused by dam failures on realistic three-dimensional terrain. The developed tool contributes to improved risk analysis, emergency planning, and safety assessment of hydraulic structures.

Keywords: numerical simulation; dam break; computational fluid dynamics; flooding; free surface; 3D terrain; Navier-Stokes equation; water resource; mathematical modelling.

Received: 10.12.2025 Accepted: 25.02.2026 Published: 30.03.2026

Introduction

Over the past few decades, an increase in the intensity of precipitation and rapid melting of snow caused by a sharp change in climate have become frequent causes of flooding [1, 2]. In recent years, floods have become very destructive in many areas of Kazakhstan, leading to human and economic losses. At the same time, flows caused by the destruction of dams pose a significant threat to settled crops, as the resulting strong flow can cause large-scale flooding. The flood phenomenon is of public and scientific interest worldwide, reflecting the need for scientific research to prevent the risk of flooding [3, 4].

One of the most obvious consequences is that droughts and floods have become more common and intense, making it more difficult to manage the distribution of natural water resources, which in turn affects the stability of agricultural and food production [5, 6]. A reservoir is an artificial lake with various uses, such as water storage, flood control, power generation, and irrigation. Throughout modern history, reservoirs have impacted settlements and the development of many cities. Therefore, the stable operation of a reservoir is extremely important. In addition to its usual functions, seasonal regulation of water levels and flood control operations during heavy rains affect the safety of the dam and the residents in the downstream areas [7]. However, extreme weather events have complicated the operation of reservoirs; short-term flooding in the upper reaches of a river can jeopardize the dam and exacerbate surface erosion of the slope in its watershed, leading to the accumulation of large amounts of sediment in the reservoir area, reducing its capacity and hindering its subsequent use. As a result, watershed management and reservoir improvement have become crucial for countries trying to adapt to climate change [8].

In recent years, due to the frequent occurrence of severe floods worldwide, the analysis of dam breaches has received increasing attention. The analysis of dam breach flow can be conducted through field observation, laboratory experiments, and numerical modelling. The continuous increase in computer processing speed over the past decade has made numerical modelling more efficient. Interfacial structures and large deformations of the free surface, as well as the hydrodynamics of free-surface flows, often play a significant role in many problems in the fields of environmental science, naval operations, and ocean technologies, such as assessing potential risks of dam, levee, and reservoir failures. The development of numerical methods for modelling free-surface flows has been the subject of research for several decades.

The class of particle-based methods, based on a Lagrangian framework for modelling multiphase flows, includes the hydrodynamics of smoothed particles [9–10], the meshless finite element method [11], and the particle finite element method [12]. These methods have been extended by many researchers to model a wide range of problems related to complex interactions between liquids and solids, due to their simplicity and high computational efficiency [13, 14]. However, these methods have some limitations, such as instability for large domains, which can lead to low accuracy and convergence issues. For Eulerian approaches, the level set method was proposed in [15, 16], and many advanced developments of this numerical method have been suggested for more accurate modelling of multiphase flows [17, 18]. Level set methods are simple but less accurate, and reinitialization methods are used to improve their accuracy. Alternatively, Volume-of-Fluid (VOF) methods, such as the piecewise linear interface calculation algorithm [19], and the least-squares interface reconstruction algorithm [20, 21], are well-known for their reasonable mass conservation and are frequently used by researchers for flow prediction [22, 23]. With the advancement of computing technology, the VOF method has been applied to model many real engineering problems [24], including large-scale engineering problems [25]. These grid-based methodologies are notable for their enhanced ability to handle flows with steep gradients over dry layers. Research into real dam breach scenarios is particularly challenging due to the scales and complex topography involved. However, it is worth noting the work, which studied flooding in an urban area due to a potential dam failure at the Urkmez dam in Izmir, Turkey [26]. This work provides an assessment of the flow propagation after a dam breach, including flood time,

inundation depth, etc. Additionally, the results of the hydrodynamic model were validated using experimental data from the physical model of the Urkmez dam breach, including the city of Urkmez.

A series of works has systematically validated VOF-based CFD against laboratory experiments, demonstrating its superior accuracy in resolving free-surface dynamics. Simsek and Islek performed 2D and 3D simulations of dam-break flows with varying upstream/downstream depth ratios and obstacle shapes using ANSYS Fluent. They compared multiple turbulence closures (RNG k-ε, SST k-ω, DES) in 2D against LES in 3D and concluded that the 3D LES-VOF model provides the best agreement with experimental water-surface profiles, especially for wave deformation and curvilinear trajectories [27]. Similarly, Esmaeeli Mohsenabadi et al. employed OpenFOAM with VOF to investigate the initial stages of dam-break propagation in both dry- and wet-bed conditions, including a trapezoidal bottom obstacle [28]. Their evaluation of RANS models (realizable k-ε, SST k-ω) highlighted the capability of VOF to accurately reproduce reflected waves and early-stage hydrodynamics within the first 1–7 seconds after failure. Coupled extensions have also emerged to address sediment-laden flows. Qiu et al. introduced a CFD-DEM model integrated with VOF to simulate cascade dam-break floods in earth-rock reservoirs, successfully reproducing particle–fluid interactions, sediment concentration effects, and downstream reservoir inundation under varying dam spacing and slope conditions [29]. Beteille et al. further validated VOF for dam-break propagation over multiple obstacle configurations, confirming its robustness for urban-like or complex-bed scenarios [30].

In the present study, the Volume of Fluid (VOF) method was adopted to simulate the dam-break flow at the Tasotkel reservoir. The primary reason for this choice is that VOF provides a highly accurate and mass-conserving tracking of the free-surface interface, enabling detailed resolution of interface evolution, wave deformation, breaking, and splashing as the flood propagates over complex real topography. Unlike conventional shallow water models (depth-averaged Shallow Water Equations), which rely on hydrostatic pressure assumptions and struggle with strongly three-dimensional effects, vertical accelerations, and non-hydrostatic pressures — particularly in the near-field of the dam and over steep or irregular terrain — the VOF approach solves the full three-dimensional Navier–Stokes equations. This results in significantly more realistic reproduction of flow features such as flow acceleration on slopes, wave distortion by bed irregularities, and lateral spreading in valleys. Compared to meshless particle methods such as Smoothed Particle Hydrodynamics (SPH), the VOF technique offers superior numerical stability on structured or unstructured meshes, better handling of complex boundary conditions, and more precise interface sharpness with minimal numerical diffusion when combined with appropriate reconstruction schemes. These capabilities are especially advantageous in the current work, as they fully exploit the high-fidelity three-dimensional terrain geometry developed specifically for this study. The novel geometry-generation workflow produces a realistic, watertight representation of the Tasotkel downstream region. The VOF method's compatibility with such detailed 3D topography allows the model to naturally capture the intricate hydrodynamic interactions between the advancing flood wave and the actual terrain, thereby demonstrating the practical value and effectiveness of the proposed geometry-construction approach for real-world dam-break simulations. This selection of the VOF method not only enhances the physical realism of the predicted inundation patterns, arrival times, and local velocities but also strengthens confidence in applying the model for hydraulic risk assessment in regions with complex terrain.

Despite many scientific advances, floods still remain a global threat. In practical applications of hydraulic engineering, accurate numerical analysis of dam-break flows must account for both river floods and floodplain inundations and be applicable to real river systems with sufficiently high spatial and temporal resolution. To better understand the dynamic characteristics of dam-break flows, it is necessary to consider the effect of flow interaction with real terrain features. In this study, the breach of the Tasotkel reservoir was simulated on actual complex terrain. A numerical model was used to simulate the flow based on the Navier-Stokes

equations. The accuracy of the numerical method is validated through two laboratory dam-break scenarios.

The present work contributes to the field of dam-break flood modelling through the following key novelties:

- Novel methodology for generating high-fidelity complex terrain geometry.
- New recommendations for systematic validation of dam-break models.
- First detailed numerical simulation of a dam-break scenario in the Tasotkel reservoir region.

Methods and Materials

The dynamics of fluids can be described using the Navier-Stokes equations. The governing equations are the three-dimensional continuity equations and the Reynolds-averaged Navier-Stokes (RANS) equations for incompressible flows of two immiscible phases, which can be expressed in the following vector form:

$$\nabla u = 0 \tag{1}$$

$$\frac{\partial u}{\partial t} + (\nabla u)u = \frac{1}{\rho} f - \frac{1}{\rho}\nabla p + \frac{1}{\rho}\nabla(\mu \nabla u) \tag{2}$$

$$\frac{\partial \chi}{dt} + u\nabla\chi = 0 \tag{3}$$

where u is the flow velocity, t is time, p is pressure, ρ is the water density, f represents external body forces, μ is the dynamic viscosity, and χ is the phase indicator. The external body force considered in this case is gravity.

To improve the numerical stability and convergence of the simulation, the VOF method was used. The motion of the water surface is captured using the Volume of Fluid (VOF) method. In this method, defining the interface between phases plays a crucial role. According to the main idea of the method, a scalar quantity is assigned to each computational cell, representing the fraction of the cell occupied by one phase, such as water.

- If this value is 0, the cell is empty.
- If it is 1, the cell is completely filled.
- If it lies between 0 and 1, the cell contains the interfaces between phases.

In other words, the volume fraction of water, α, is defined as the ratio of the volume of water in the cell to the total volume of the cell. Accordingly, the value 1−α represents the volume fraction of the second phase in the cell, such as air.

The temporal evolution of α is described by the transport equation:

$$\frac{\partial \alpha}{\partial t} + \frac{\partial(\alpha \overline{u_i})}{\partial x_i} = 0 \tag{4}$$

where u is the velocity field and index i represents three dimensions.

The position of the free surface is determined by equation (4). Therefore, the physical properties of the phases are averaged using the corresponding coefficients. For example, the density ρ and dynamic viscosity μ at any point are calculated as weighted averages based on the volume fraction α:

$$\rho = \alpha\rho_1 + (1-\alpha)\rho_2\,,\ \mu = \alpha\mu_1 + (1-\alpha)\mu_2 \tag{5}$$

Here, the indices 1 and 2 represent the first and second phases (water and air, respectively). These averaged properties ensure a smooth transition between the phases in the computational model.

The PISO algorithm was chosen as the numerical method for solving the presented equations. It is an extension of the SIMPLE algorithm used to solve the Navier-Stokes equations. The PISO algorithm includes a prediction step and a correction step (predictor-corrector). The algorithm can be implemented as follows:

1. Set boundary conditions.
2. Solve the discrete momentum equation to calculate the intermediate velocity field.
3. Calculate mass fluxes at the cell faces.
4. Solve the pressure equation.
5. Correct the mass fluxes at the cell faces.
6. Correct the velocities based on the new pressure field.
7. Update the boundary conditions.
8. Repeat from step 3 for the specified number of iterations.
9. Increase the time step and repeat from step 1.

After dividing the area of calculation into control volumes, the determinant equations are combined into each control volume to convert the flow variables into a system of algebraic equations. The resulting equations are solved iteratively. The momentum equation on the X-axis is expressed by the first-order upper-flow scheme:

$$\frac{u^{n+1}-u^n}{\Delta t}\Delta x\Delta y\Delta z + [(uu)_e - (uu)_w]\Delta y\Delta z + [(vu)_n - (vu)_s]\Delta x\Delta z + [(wu)_b - (wu)_t]\Delta x\Delta y = -\frac{1}{\rho}[(p)_e - (p)_w]\Delta y\Delta z + \mu[((\frac{\partial u}{\partial x})_e - \left(\frac{\partial u}{\partial x}\right)_w)\Delta y\Delta z + ((\frac{\partial u}{\partial y})_n - \left(\frac{\partial u}{\partial y}\right)_s)\Delta x\Delta z + ((\frac{\partial u}{\partial z})_b - \left(\frac{\partial u}{\partial z}\right)_t)\Delta x\Delta y]. \quad (6)$$

The momentum equation on the Y-axis is expressed by the first-order upper-flow scheme:

$$\frac{v^{n+1}-v^n}{\Delta t}\Delta x\Delta y\Delta z + [(uv)_e - (uv)_w]\Delta y\Delta z + [(vv)_n - (vv)_s]\Delta x\Delta z + [(wv)_b - (wv)_t]\Delta x\Delta y = -\frac{1}{\rho}[(p)_n - (p)_s]\Delta x\Delta z + \mu[((\frac{\partial v}{\partial x})_e - \left(\frac{\partial v}{\partial x}\right)_w)\Delta y\Delta z + ((\frac{\partial v}{\partial y})_n - \left(\frac{\partial v}{\partial y}\right)_s)\Delta x\Delta z + ((\frac{\partial v}{\partial z})_b - \left(\frac{\partial v}{\partial z}\right)_t)\Delta x\Delta y]. \quad (7)$$

The momentum equation on the Z-axis is expressed by the first-order upper-flow scheme:

$$\frac{w^{n+1}-w^n}{\Delta t}\Delta x\Delta y\Delta z + [(uw)_e - (uw)_w]\Delta y\Delta z + [(vw)_n - (vw)_s]\Delta x\Delta z + [(ww)_b - (ww)_t]\Delta x\Delta y = -\frac{1}{\rho}[(p)_b - (p)_t]\Delta x\Delta z + \mu[((\frac{\partial w}{\partial x})_e - \left(\frac{\partial w}{\partial x}\right)_w)\Delta y\Delta z + ((\frac{\partial w}{\partial y})_n - \left(\frac{\partial w}{\partial y}\right)_s)\Delta x\Delta z + ((\frac{\partial w}{\partial z})_b - \left(\frac{\partial w}{\partial z}\right)_t)\Delta x\Delta y] + g\Delta x\Delta y\Delta z. \quad (8)$$

To solve the dependence of pressure on velocity in the Navier-Stokes equations, the Presto method is used. In the PRESTO scheme, the pressure field is relative to the velocity field, which means that the pressure values are located in the Centers of the calculation cells, and the velocity values are located on the surfaces of the cells. With PRESTO, the following final volume expression can be used to sample the pressure term in the Navier-Stokes equations:

$$(\nabla \mathrm{P})_E = \nabla \mathrm{P}_c + \propto \nabla \mathrm{P}_f. \quad (9)$$

The values of the pressure exerted by the specified methods determine the values of the speed components in the new time step. These defined new values are used to describe the equations remaining in the next iteration. The equation describing the phase is summarized as follows:

$$\frac{\alpha_q^{n+1}\rho_q^{n+1}-\alpha_q^n\rho_q^n}{\Delta t}\Delta x\Delta y\Delta z + [(u\alpha\rho)_e - (u\alpha\rho)_w]\Delta y\Delta z + [(v\alpha\rho)_n - (v\alpha\rho)_s]\Delta x\Delta z + [(w\alpha\rho)_b - (w\alpha\rho)_t]\Delta x\Delta y = 0. \quad (10)$$

n+1 – new (current) time step index;
n – index of the previous time step;
V – cell volume;
A_f – area on the corresponding face of cell;
F_f, F_e, F_w, F_n, F_s, F_t, F_b – convective flows on the corresponding surfaces;
P_f – interpolated pressure values on the corresponding surfaces.

Model Verification

In the test case, we evaluated the developed model for water flow over a trapezoidal-shaped step. The purpose of this test is to demonstrate the movement of the flow over the bottom topography. The obtained numerical results are compared with the experimental data from Kocaman (2007) to verify their accuracy [31], as well as with numerical results from [32, 33] by Marsooli and Wu (2014) and Ozmen-Cagatay and Kocaman (2011). The geometry of the first study area, where the calculations were performed, is shown in Figure 1, which also indicates the origin of the coordinate system.

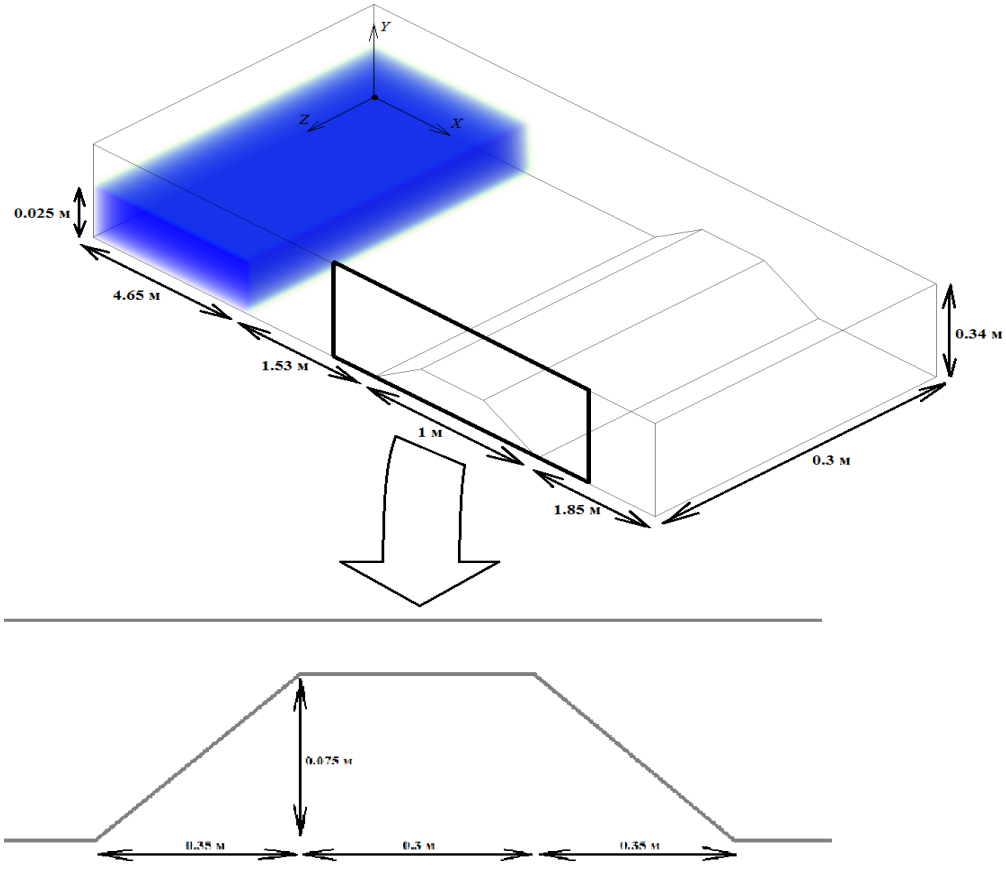

Figure 1. Geometry of the first test case with a trapezoidal step.

The boundaries of the reservoir at x=9.03 m and y=0.34 m are considered open, while all other boundaries are impermeable walls. Figure 2 presents the obtained wave contour results at specific time moments (t=1.9 s, t=2.8 s, t=3.3 s, t=3.68 s, t=4.74 s, t=6.68 s). These graphs have been dimensionless using the initial water height at t=0. The origin of the x-axis in the graphs corresponds to the coordinate position of the gate that initially held the water.

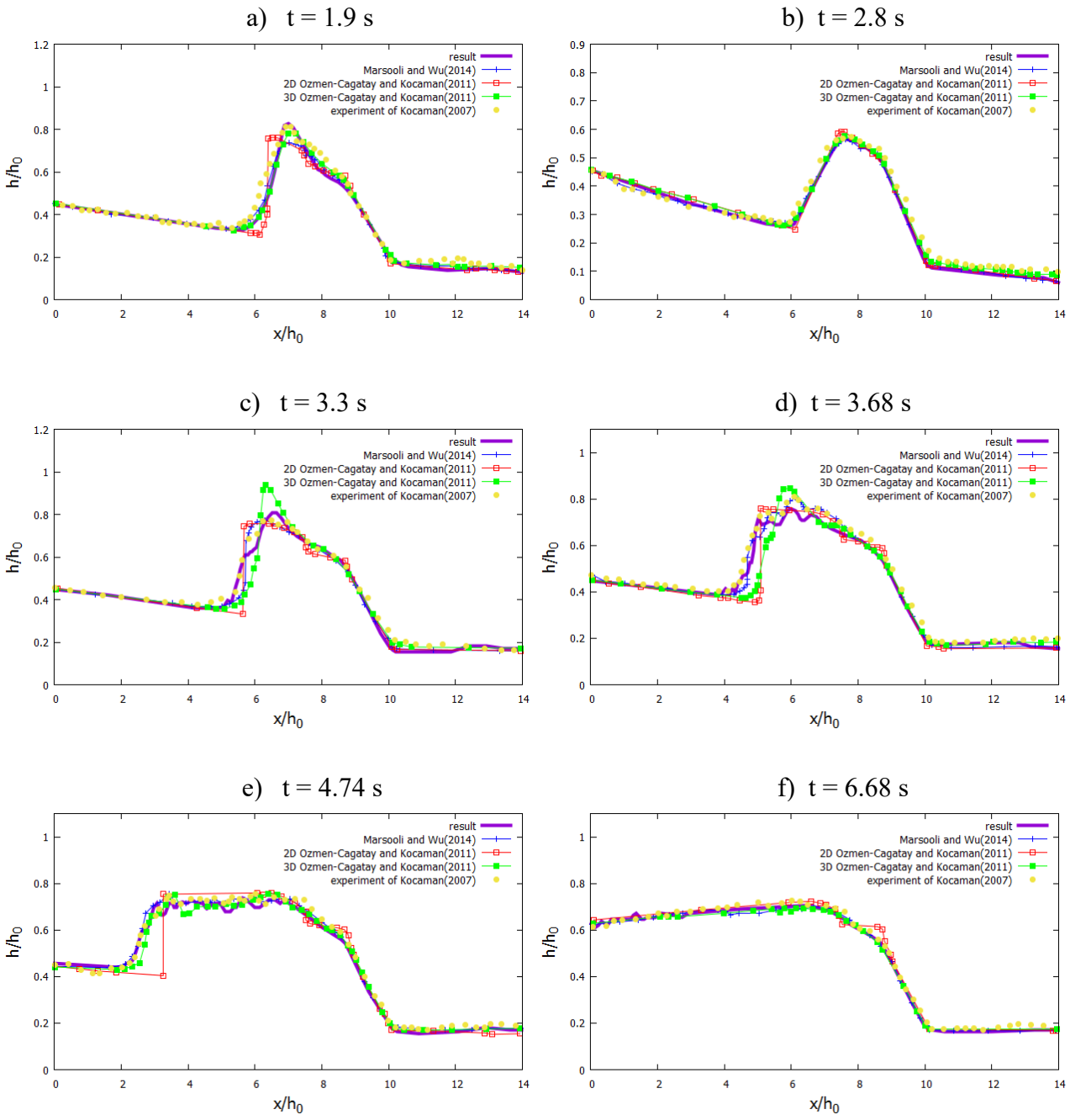

Figure 2. Water level height graphs at different time moments.

From the results in Figure 2, it is also evident that the proposed numerical model accurately predicts the behavior of the breakthrough flow at different time moments. Figures 3 and 4 present the two-dimensional and three-dimensional flow contours after the dam break.

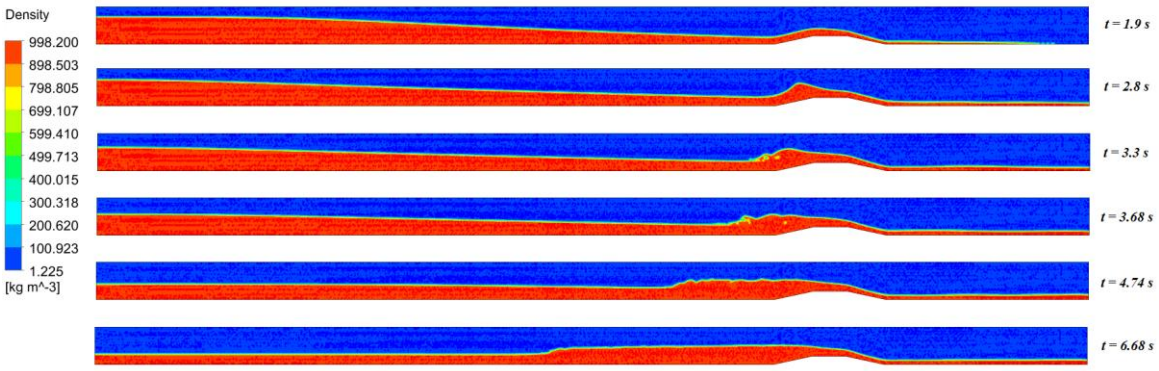

Figure 3. Two-dimensional wave contours.

As expected, the results presented in Figure 3 show that the bottom topography of the study area significantly slows down the flow velocity. However, at the same time, the water level in this area increases, leading to a higher degree of flooding.

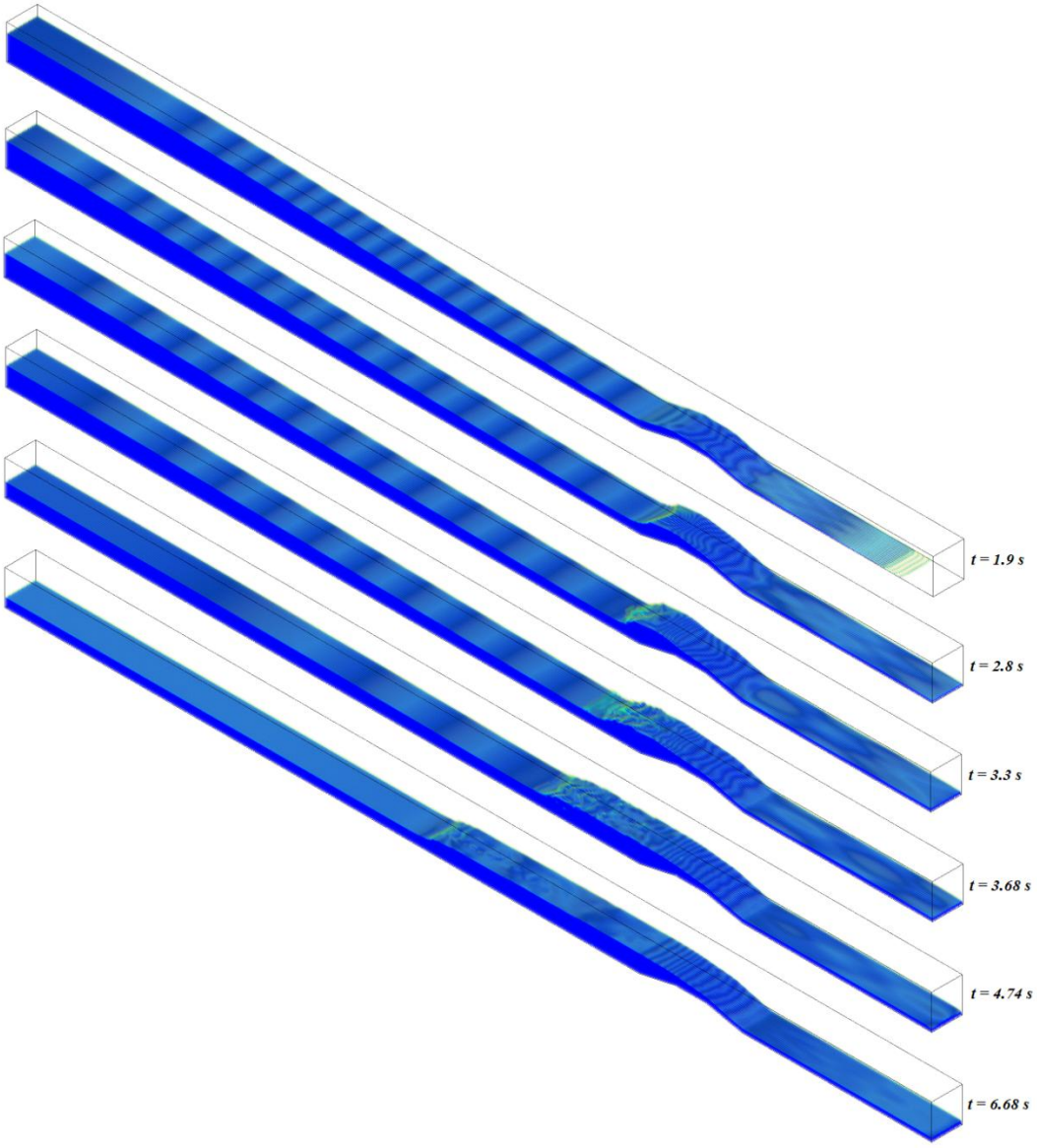

Figure 4. Three-dimensional wave contours at different time moments.

As shown in Figure 4, at t=1.9 s, the water completely covers the step. Then, the wave height increases, and at t=2.8 s, the water begins to reflect and move backward. Additionally, at t=1.9s, t=2.8 s, and t=6.68 s, the water surface remains smooth, and the computed values are very close to the experimental data. However, at t=3.3 s and t=3.68 s, small waves and vortices form on the surface, making it more turbulent, which may lead to minor discrepancies. The comparison in Table 1 indicates that the applied model yields results that closely match real-world observations.

Table 1. Deviation values of numerical calculations from laboratory data.

Comparison variables	Error %	RMSE
Water level height	4.3	0.007351562 m

The proposed mathematical model and numerical methods were validated by comparing its numerical outputs with a second experimental dataset. The experiment was carried out at the State Key Laboratory of Hydraulics and Mountain River Engineering, Sichuan University, and the geometric parameters used in the simulations matched those of the experiment [34]. The experimental setup is illustrated in Figure 5.

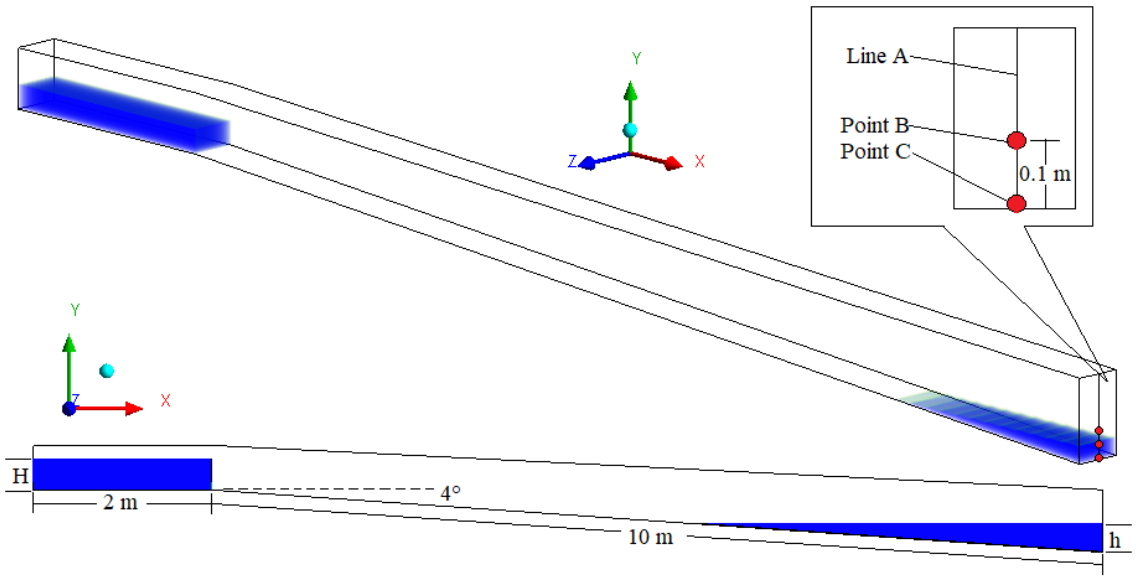

Figure 5. Geometry of the experimental setup with inclination.

The computational model consisted of a straight channel with a 4° bed slope. The upstream and downstream dams were separated by a distance of 10 m, and the channel had a rectangular geometry with a width of 0.4 m. The initial water depth at the upstream dam is defined as H, whereas the depth at the downstream dam is referred to as h. A comparison of the numerical results with the experimental data is presented in Figure 6.

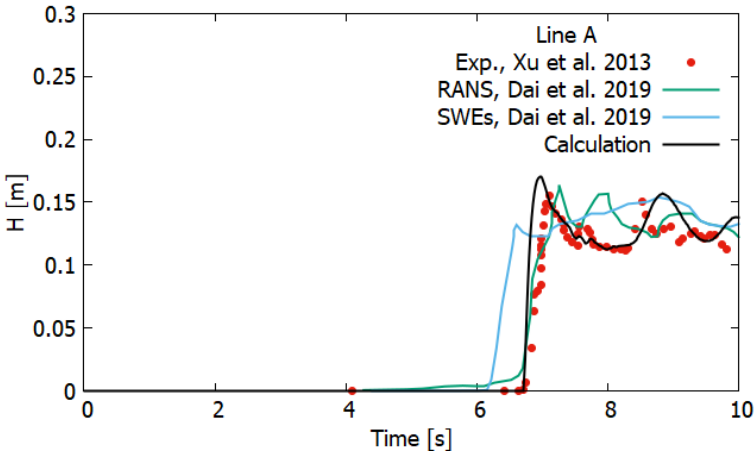

Figure 6. Water level along measurement line A at different time moments.

The water depth in cascading reservoirs plays a crucial role in shaping the evolution of dam-break flow. As shown in Figure 6, when the downstream reservoir is initially empty, a gradual rise in water level occurs as the dam-break wave travels along the channel. The black curve represents the numerically predicted water surface elevation downstream, while the red curve corresponds to the experimental measurements. Numerical results from alternative modeling approaches reported by other authors are also included in Figure 6 for comparison.

As the breach wave propagates, it fills the lower reservoir and, due to its high kinetic energy, rapidly advances downstream along the free surface. At approximately 7 seconds, the wave front reaches the lower reservoir, triggering an abrupt increase in the water level. With the continuous inflow from upstream, a recirculating motion develops and becomes noticeable from around 8 seconds onward. By 10 seconds, the water level in the upper reservoir begins to drop, leading to a decline in the discharge rate. Figure 7 shows the comparison between numerical and experimental results.

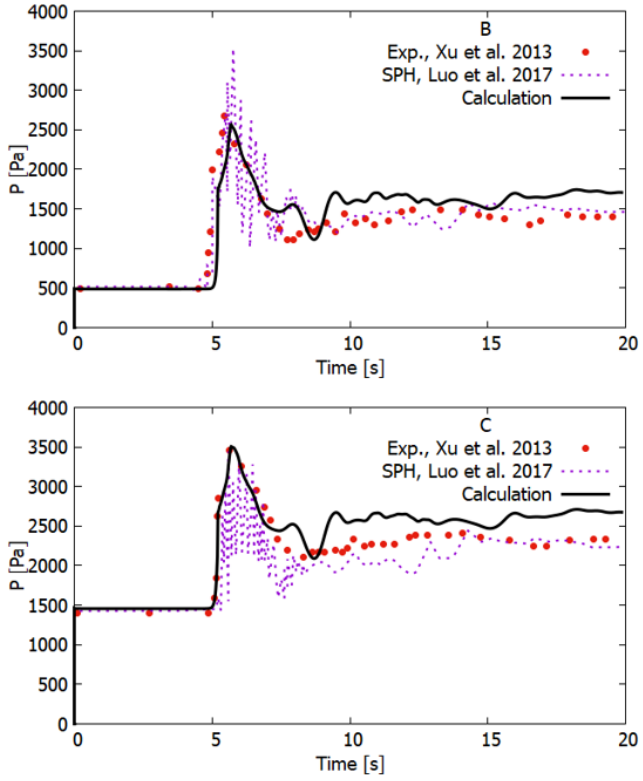

Figure 7. Pressure profiles at measurement points B and C.

Based on the presented results, the influence of a dam-break wave acting on an inclined surface can be interpreted as a two-stage process involving both dynamic and quasi-static effects. The first stage is dominated by a high-velocity surge, during which the rapidly advancing flow exerts an impulsive force on downstream structures. This sudden impact may be sufficient to trigger immediate failure of the next dam in a cascading reservoir system, particularly when the structure lacks adequate resistance to dynamic loading. The second stage involves a gradual increase in pressure as the reservoir begins to fill and oscillatory motions become established. Unlike the initial shock, this phase is characterized by fluctuating water levels and cyclic forces that act over a prolonged period. These oscillations can induce fatigue, instability, or progressive deterioration of the downstream dam, ultimately leading to structural damage even if the initial impact did not cause collapse. Therefore, both mechanisms, the instantaneous dynamic load and the sustained oscillatory pressure, must be considered when assessing dam safety, designing protective measures, or analyzing the hydraulic response of cascading reservoirs under dam-break conditions. Figure 8 shows snapshots of the water flow, demonstrating the impact of the dam-break process on channel flow at different time instances.

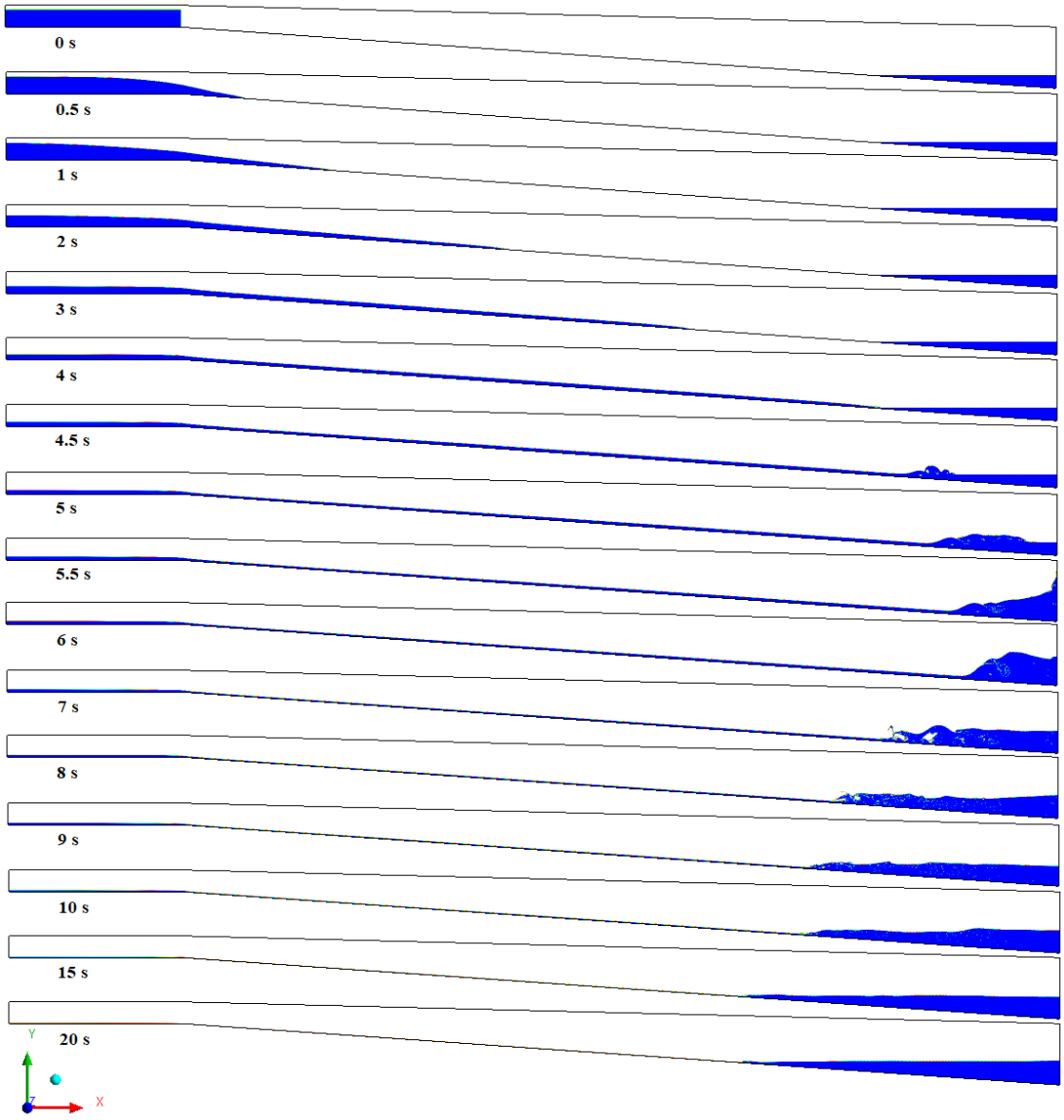

Figure 8. Snapshots of the dam break at different time moments.

The abrupt nature of flooding becomes particularly evident when a non-zero water depth exists in the downstream section of the channel. In such cases, the dam-break wave produced upstream forces the lower reservoir to transition from an initially quiescent state into a highly dynamic environment. As illustrated in Figure 8, once the upper dam fails, the advancing surge interacts with the pre-existing downstream water body. Upon reaching the lower reservoir, the rapidly propagating flow encounters hydraulic resistance at the downstream dam, resulting in the formation of a pronounced backflow wave at approximately 4.5 seconds.

During the period from 5 to 8 seconds, the hydrodynamic conditions intensify, and the flow field becomes strongly turbulent. A reverse flood wave develops and travels upstream, indicating a significant redistribution of momentum within the reservoir. At this stage, the flow structure exhibits a clear two-layer behavior: surface water continues to move downstream under the influence of inertia, while bottom water is driven upstream by the reflected surge. This produces a highly turbulent, recirculating motion, consistent with the complex interaction between incoming and standing waters in cascading systems. Based on the comparison presented in Table 2, it can be concluded that the applied model produces results that are highly consistent with real-world observations.

Table 2. Deviation values of numerical calculations from laboratory data.

Comparison variables	Error %	RMSE
Height A	5.89	0.00673 м
Pressure B	8.98	153.737 Па
Pressure C	7.42	209.726 Па

The results confirm that the proposed numerical model is capable of accurately reproducing such complex hydraulic processes. Its successful validation across three independent test cases with varying topographic conditions highlights its robustness and applicability. Consequently, the model will be further employed to analyze dam-break phenomena over real-world terrain configurations, offering valuable potential for practical risk assessment, flood forecasting, and design optimization in hydraulic engineering.

Results

For the purpose of modeling a real dam-break scenario, the Tasotkel Reservoir was selected as a case study. The reservoir, with a total storage capacity of approximately 1.0 billion m^3, is located in the Zhambyl region of Kazakhstan. It was constructed on the Chu River and serves as an important water body for irrigation, hydropower generation, and flood regulation in the region. The earthen embankment dam of Tasotkel has a height of about 50 meters and a crest length of nearly 1,000 meters. The surrounding terrain is represented by broad steppe valleys with relatively gentle slopes. Due to its considerable storage volume and strategic importance for water management, Tasotkel Reservoir poses significant potential consequences in the event of a dam-break scenario. A satellite image of the reservoir and its surroundings is presented in Figure 9.

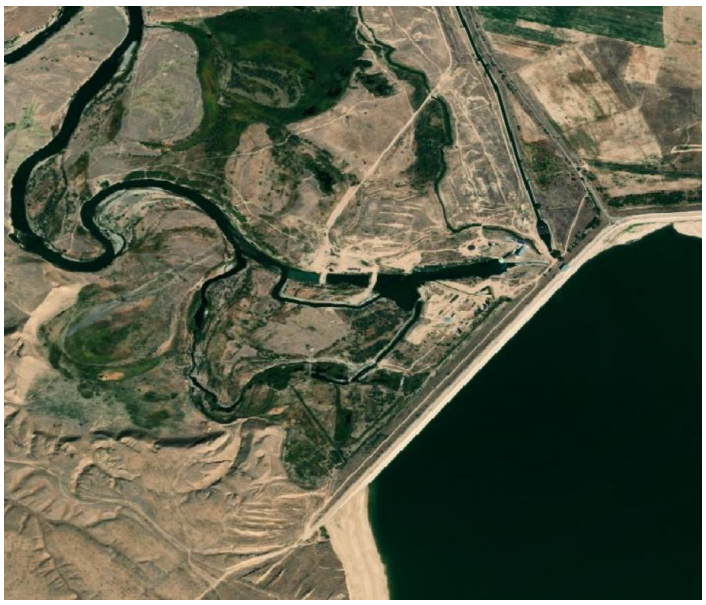

Figure 9. Satellite image of the Tasotkel Reservoir.

To study the dam-break flow on a real three-dimensional mountainous terrain, the area was digitized using ArchiCAD and AutoCAD software. The ArchiCAD software package allows for the creation of a three-dimensional map using a topographic contour map, as shown in Figure 10.

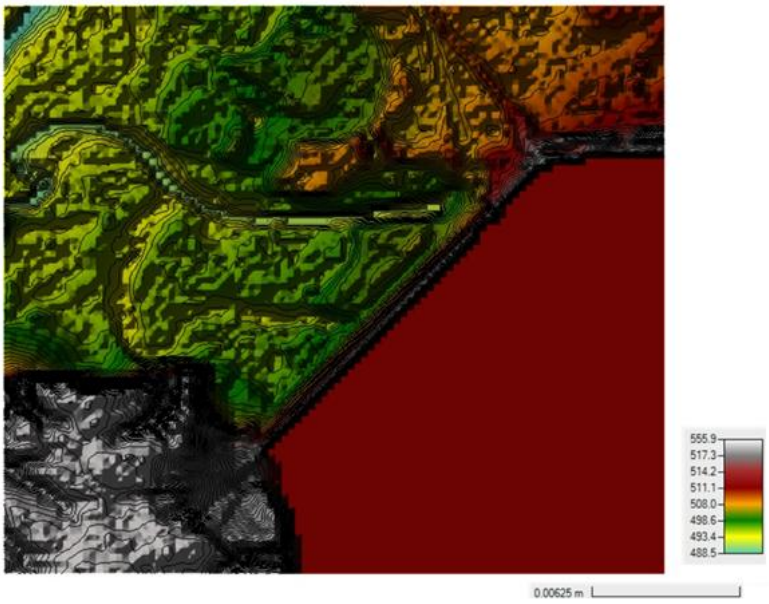

Figure 10. Contour isomap of the Tasotkel Reservoir.

The digitized data from Figure 10 are transformed into a three-dimensional terrain model, as shown in Figure 11. The three-dimensional terrain geometry obtained from Figure 10 is modified into the bottom topography of the study area using the AutoCAD software package. To ensure efficient numerical simulation, unnecessary parts of the study area were removed.

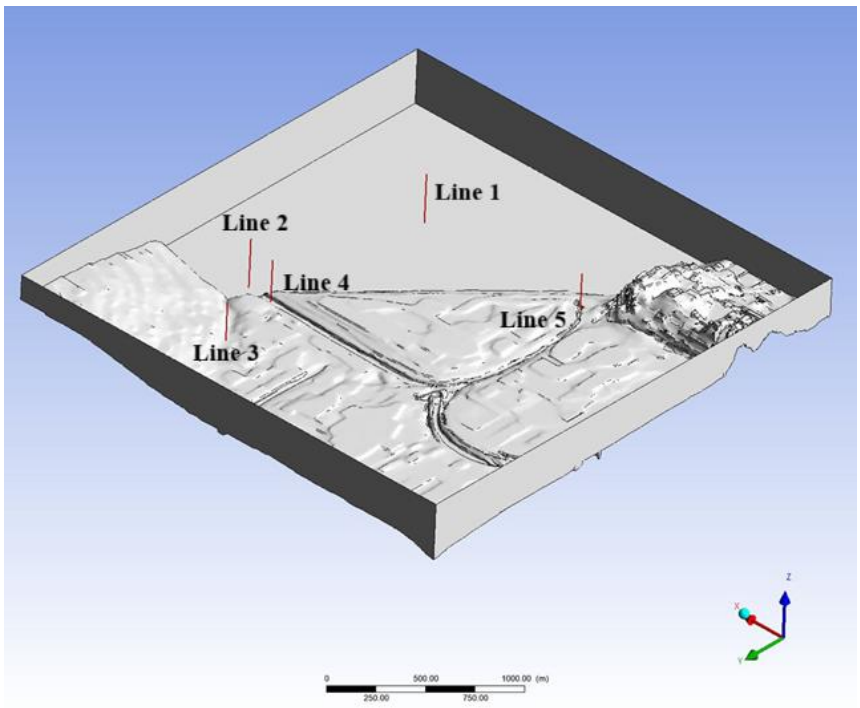

Figure 11. Three-dimensional terrain of the Tasotkel Reservoir.

Figure 11 presents the final three-dimensional geometry of the Tasotkel's region terrain with dimensions of 2927 × 2861 × 332 meters. The computational grid, refined towards the bottom, consisted of 1243756 elements. In all numerical calculations, the initial condition was given as follows: $t = 0$; $u = 0$; $P = 0$. Boundary conditions on the open (outlet) boundaries of the computational domain: $\partial u/\partial n = 0$; $P = 0$. Boundary conditions on the closed boundaries of the computational domain were as follows: $u = 0$; $\partial P/\partial n = 0$, where n denotes the normal direction. A reservoir with an approximate water volume of 0.2145 km³ is located in the upper part of the study area, as shown in Figure 12. In the discretization scheme used, the time and spatial steps are expressed through the Courant number to ensure stability. This condition arises from the requirement that the change in the variables describing the flow should not propagate faster than the flow velocity. In our calculations, the Courant number was taken as 0.25.

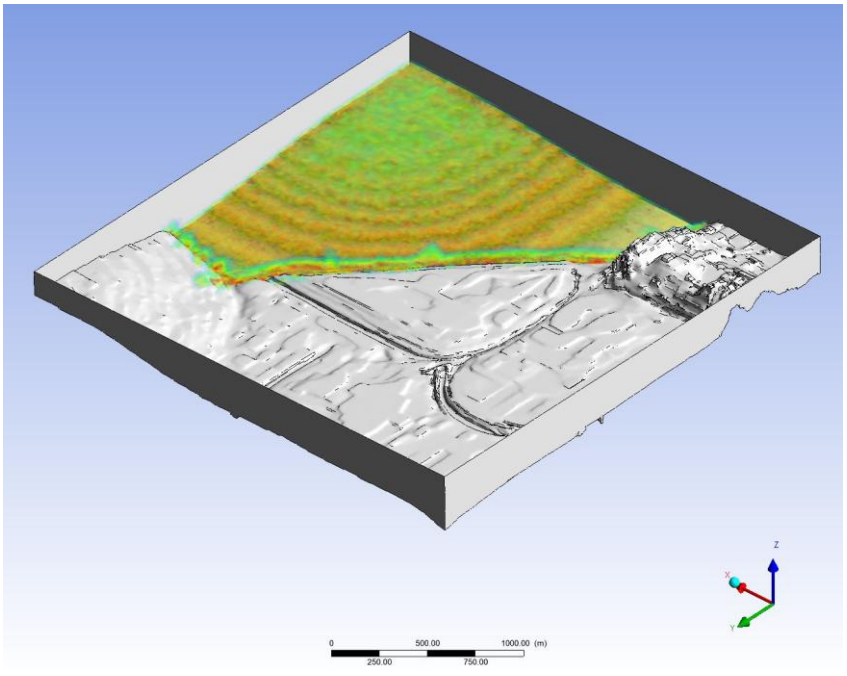

Figure 12. Setup of the real three-dimensional problem.

As shown in Figure 12, the failure of the Tasotkel Reservoir is assumed, causing a large volume of water to flow down the local terrain due to gravity. The dam-break scenario considered in this study represents a hypothetical instantaneous failure of the Tasotkel dam. For the purpose of numerical simulation, the actual dam structure was entirely removed from the computational domain to simulate the worst-case sudden release of the impounded water into the downstream valley. At the initial time (t = 0 s), the computational domain contains a stationary water column corresponding to the full reservoir level with 120 m water depth, while the entire downstream region is considered a dry bed (or with negligible initial water depth). Gravity is activated as the driving force, allowing the water to flow suddenly into the downstream area under the influence of the hydrostatic pressure difference. This setup mimics the classical instantaneous dam-break problem but applied to a real, complex topographic domain rather than idealized channels. The VOF method is employed to track the dynamic evolution of the water–air interface as the flood wave propagates over the irregular terrain. The scenario enables detailed investigation of key hydrodynamic features, including the initial wave front acceleration, interaction with bed structures and topographic obstacles, wave deformation due to channel inclination and roughness, flood inundation extent, and arrival times at critical downstream locations.

To ensure the numerical results are not sensitive to the computational grid resolution, a mesh independence study was conducted. As shown in Figure 13, a series of meshes with varying element sizes were evaluated, ranging from coarse to fine resolutions.. Key output velocity magnitude was monitored at selected locations.

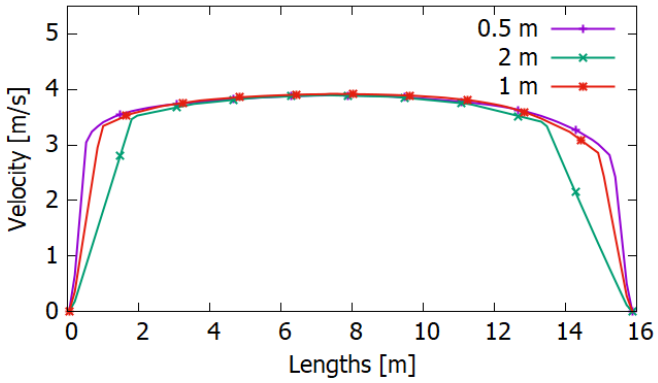

Figure 13. Velocity profiles in the Chu River for the different mesh sizes..

The results showed minimal variation between the two finest meshes, indicating convergence of the solution with respect to grid refinement. Based on a balance between accuracy and computational cost, the mesh with 1243756 elements and a minimum cell size of 1 m was selected for all subsequent simulations. All simulations were performed under transient, three-dimensional conditions with appropriate turbulence modeling to capture the highly unsteady and turbulent nature of the flow. For observation, Figure 14 presents three-dimensional simulation snapshots at different time moments.

b) t = 10 s b) t = 20 s

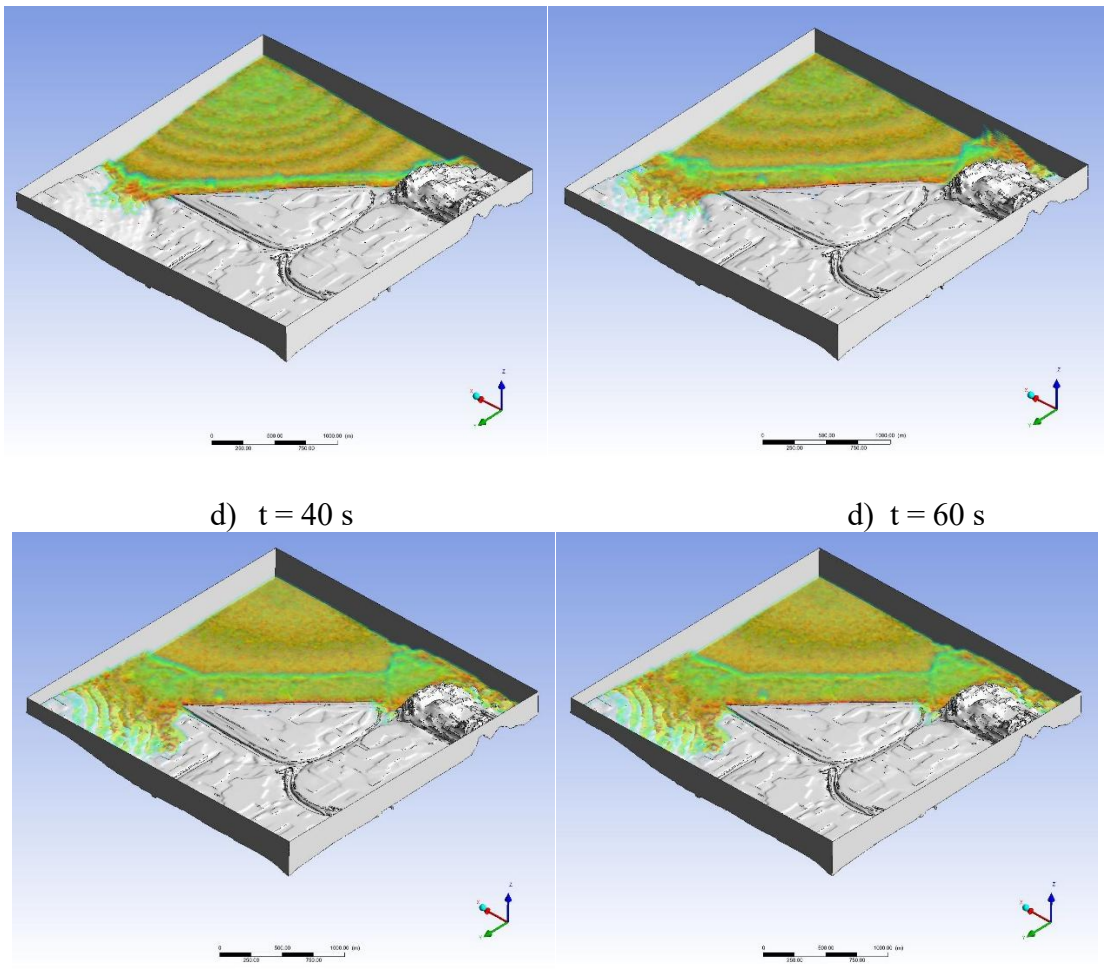

Figure 14. Three-dimensional simulation snapshots for Tasotkel reservior.

Figure 14 presents the behavior of the dam-break flow at different time moments on the actual terrain. These results show that the flow forms a river current along the Chu River, confirming the accuracy of the digitized complex terrain geometry. Additionally, Figure 15 presents the results for measurement lines 1–5.

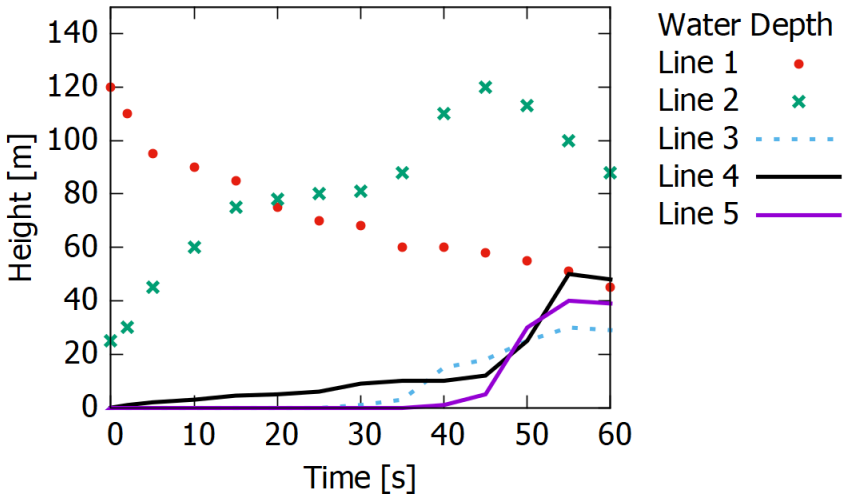

Figure 15. Flow height profiles at the measurement lines.

The results in Figure 15 illustrate how the flow height changes at different locations within the study area (lines 1–5). As expected, the water level at line 1 gradually decreases and reaches a

more stable state after 30 seconds. The dam-break flow reaches the edge of the study area at 55 seconds after the breach. This indicates that the Tasotkel Reservior failure could cover an approximate distance of 1 km in 55 seconds, with an average velocity of 18.2 m/s. It is important to note that such a powerful flow, with a height of 25 meters, could cause significant damage to the region. Figure 14 also presents the flooding levels along estuaries measurement lines 4–5, where the arrival time of the flow can be observed. Oscillations are noticeable at all measurement lines, which are attributed to the irregular flow behavior caused by the complex terrain geometry, leading to turbulent flow. Another possible reason for these oscillations is the computational grid of the study area. Thus, the proposed modeling approach has demonstrated its reliability for 3D dam-break simulations and can serve as an alternative for investigating practical hydraulic engineering problems.

Discussion

The numerical simulations conducted for the Tasotkel reservoir demonstrate that the applied VOF-based approach effectively captures the dynamics of dam-break flows over complex terrain. The observed propagation patterns, flood extents, and interface evolution are consistent with findings reported in previous studies investigating free-surface flows and inundation processes on irregular topography, which strengthens confidence in the adopted methodology. The model's ability to reproduce dam break scenarios, including dam breaks in trapezoidal and inclined channels, aligns with comparable validation approaches in the literature, where simplified domains are used to test the numerical stability and physical realism of flood models. These results indicate that the proposed approach performs reliably under both idealized and realistic conditions.

The first notable novelty of the present work lies in the systematic validation using two complementary benchmark experiments prior to the real-terrain application. The first test demonstrates how bed structure (including irregularities and roughness elements) influences flow resistance, wave deformation, and overall propagation behavior. The second test illustrates the significant role of channel inclination in accelerating or decelerating the flow, altering water movement, and modifying the flood front evolution. This dual-validation strategy is essential for reliable simulation of water flows in real terrain, as it ensures the model accurately accounts for the combined effects of topographic complexity and slope-driven hydrodynamics—factors that are often oversimplified or tested in isolation in conventional dam-break studies.

The most innovative aspect of the present work lies in the methodology developed for constructing a high-fidelity geometric model of the actual Tasotkel reservoir region suitable for three-dimensional CFD analysis. High-resolution satellite imagery was first utilized to generate an isomap of the terrain. This was then imported into ArchiCAD, which proved to be an excellent tool for creating a realistic 3D terrain surface. The resulting geometry was subsequently transferred to AutoCAD for precise corrections, removal of unnecessary surrounding areas, and final preparation as a clean, watertight model ready for CFD import. The combination of ArchiCAD's strong capabilities in terrain generation and AutoCAD's precision in geometry editing and refinement allowed the creation of a terrain representation that closely mirrors real-world topographic features. This practical workflow addresses a common challenge in applying advanced VOF-based models to real dam-break scenarios and provides a reproducible pathway for similar studies in regions with complex terrain.

The present results demonstrate that the VOF-based multiphase approach not only accurately tracks the large-scale deformation and propagation of the free surface but also effectively captures the complex hydrodynamic interactions between the advancing flood wave and the three-dimensional irregular terrain. This capability is particularly valuable because it allows the model to reproduce key physical mechanisms such as flow acceleration over steep slopes, deceleration and wave distortion due to topographic obstacles, lateral spreading in valleys,

and the formation of secondary currents—phenomena that are difficult to predict using simplified 1D or 2D models. From a practical perspective, these findings have important implications for hydraulic risk assessment and emergency planning. By providing spatially distributed predictions of inundation extent, maximum water depths, and local flow velocities over real topography, the model enables a more reliable identification of high-risk zones and vulnerable downstream settlements and infrastructure in the Tasotkel region. Such detailed information is essential for developing accurate flood hazard maps and designing effective mitigation measures.

Nevertheless, the simulations also highlight several inherent limitations of the current methodology. Small-scale terrain features (e.g., narrow gullies, local depressions, or micro-topography) are not always fully resolved due to mesh constraints, which can lead to underestimation or overestimation of localized energy dissipation and wave damping. Furthermore, the model does not yet account for movable-bed processes, including sediment entrainment, transport, and deposition, all of which can significantly alter flood wave celerity, inundation patterns, and final deposition zones during a real dam-break event. Although the dual validation against idealized trapezoidal and inclined-channel experiments shows good quantitative agreement with reference data, the transition to a fully realistic terrain introduces additional uncertainties related to topographic data accuracy and surface roughness parameterization. Therefore, future work should focus on further calibration and validation using available field measurements or post-event survey data from analogous events to improve model reliability and reduce predictive uncertainty in real-world applications.

Conclusion

Overall, the three-dimensional dam-break modeling of the Tasotkel reservoir over real terrain confirms the effectiveness and practicality of numerical investigation for complex hydraulic problems. The simulations accurately reproduced key hydrodynamic characteristics, including the arrival time of the surge front and the inundation levels downstream of the breach. The reliability of the numerical approach was verified through comparison with two independent laboratory experiments. In all cases, the agreement between numerical predictions, experimental observations, and results reported by other researchers was strong, reinforcing the validity of the methodology.

A minor discrepancy was identified during the initial stages of the dam-break event, where the simulated water surface elevation slightly deviated from experimental measurements. This variation is expected, as the physical conditions in real terrain differ from controlled laboratory settings, making exact coincidence between numerical and experimental results inherently difficult. Nevertheless, the proposed method successfully captured the evolution of the free-surface flow without exhibiting numerical instability, and it was capable of resolving transitions between subcritical, supercritical, and mixed-flow regimes.

Beyond validation, the results highlight the model's capability to handle realistic geomorphology, suggesting significant applicability for flood assessments in natural river networks with irregular topography and heterogeneous floodplain characteristics. Therefore, the study demonstrates the potential of the presented computational framework as a robust quantitative tool for dam-break analysis, flood hazard evaluation, and decision-support in flood risk management.

Acknowledgement

This research was funded by the Science Committee of the Ministry of Science and Higher Education of the Republic of Kazakhstan, grant number BR24993128 "Information-analytical system development for the transboundary water resources effective use in the Zhambyl region agricultural sector."

References

[1] Ali A., Stephen J.U., Salisu D.S. (2026). Dam break modelling and flood inundation mapping using GIS and HEC-RAS: a case study of the Tiga Earth dam, Kano State, Nigeria. Water Sci Technol, 92 (12): 1687–1708. https://doi.org/10.2166/wst.2025.172

[2] Bolan, S., Padhye, L.P., Jasemizad, T., Govarthanan, M., Karmegam, N., Wijesekara, H. (2024). Impacts of Climate Change on the Fate of Contaminants through Extreme Weather Events. Science of the Total Environment, 909, 168388. https://doi.org/10.1016/j.scitotenv.2023.168388

[3] Mondino, E., Scolobig, A., Borga, M. and Di Baldassarre, G. (2020). The Role of Experience and Different Sources of Knowledge in Shaping Flood Risk Awareness. Water, 12, 2130. https://doi.org/10.3390/w12082130

[4] Nabinejad, S., Schüttrumpf, H. (2023). Flood Risk Management in Arid and Semi-Arid Areas: A Comprehensive Review of Challenges, Needs, and Opportunities. Water, 15, 3113. https://doi.org/10.3390/w15173113

[5] Aznar-Crespo, P., Aledo, A., Melgarejo-Moreno, J., Vallejos-Romero, A. (2021). Adapting Social Impact Assessment to Flood Risk Management. Sustainability, 13, 3410. https://doi.org/10.3390/su13063410

[6] Littell, J.S., Peterson, D.L., Riley, K.L., Liu, Y., Luce, C.H. (2016). A review of the relationship between drought and forest fire in the United States. Glob. Chang. Biol., 22, 2353–2369. 10.1111/gcb.13275

[7] Wang, H., Wu, X., Bi, N., Li, S., Yuan, P., Wang, A., Syvitski, J.P.M., Saito, Y., Yang, Z., Liu, S., Nittrouer, J. (2017). Impacts of the dam-orientated water sediment regulation scheme on the lower reaches and delta of the Yallow River (Huanghe): a review. Glob. Planet. Chang., 157, 93–113. https://doi.org/10.1016/j.gloplacha.2017.08.005

[8] Kobayashi, S., Koshiba, T., Sumi, T. (2018). Reservoir sediment management by bypass tunnels. J. Disaster Res., 13 (4), 668–676.

[9] Naoki T., Takafumi G., Moeto W., Abbas K., Hitoshi G. (2026). Development of Interphase Particle for multiphase flow simulation by ISPH. Computational Particle Mechanics, 15, 96-111. https://doi.org/10.1016/j.cpms.2026.04.002.

[10] Agyei K.D., Zhang Q. (2026) Numerical simulation of sediment transport using a free-surface resolving Eulerian–Lagrangian approach. Physics of Fluids 38, 013343 10.1063/5.0302354

[11] Riski K., Sri R.P., Rani S. (2025). Numerical study of two-dimensional sediment transport using momentum-conserving staggered grid scheme. Journal of Computational Science, 92, 102714. https://doi.org/10.1016/j.jocs.2025.102714

[12] Fangrui L., Huai Z., Yaolin S. (2024). An open-source Boussinesq types of equations solver based on OpenFOAM. SoftwareX, 27, 101808. https://doi.org/10.1016/j.softx.2024.101808.

[13] Juan G.M., Javier C., Alberto S. (2024). Multiphase simulations of nonlinear fluids with SPH. Computational Particle Mechanics, 11, 4, 1803-1823. https://doi.org/10.1007/s40571-024-00712-3.

[14] Sun, P., Zhang, A. M., Marrone, S., Ming F. (2018). An accurate and efficient SPH modeling of the water entry of circular cylinders. Appl Ocean Res, 72, 60–75. 10.1016/j.apor.2018.01.004

[15] Saeed A.R., Shakeel A.K., Khuda B.A., Afaque A.B. (2025). Improved explicit finite difference method for extended shallow water partial differential equation. Partial Differential Equations in Applied Mathematics, 16, 101316. https://doi.org/10.1016/j.padiff.2025.101316.

[16] Pourshahbaz, H., Ghobrial, T., & Shakibaeinia, A. (2024). Evaluation of a Coupled CFD and Multi-Body Motion Model for Ice-Structure Interaction Simulation. Water, 16(17), 2454. https://doi.org/10.3390/w16172454

[17] Xu, J.; Zhang, Y.; Ma, Q.; Zhang, J.; Hu, Q.; Zhan, Y. Dam-Break Hazard Assessment with CFD Computational Fluid Dynamics Modeling: The Tianchi Dam Case Study. Water 2025, 17, 108. https://doi.org/10.3390/w17010108

[18] Maranzoni, A.; Tomirotti, M. Three-Dimensional Numerical Modelling of Real-Field Dam-Break Flows: Review and Recent Advances. Water 2023, 15, 3130. https://doi.org/10.3390/w15173130

[19] Zhao S., Yao C., Zhang W. (2026). Experimental and Numerical Investigation of Instantaneous Dam-Break Waves Under Variable Downstream Conditions. Int J Civ Eng, 24, 651–671. https://doi.org/10.1007/s40999-025-01202-0

[20] Ting Z., Yong P., Jianping M., Kuandi Z., Yunlong F. (2025). Wetting-drying scheme for discrete Boltzmann modeling of shallow water flows. Journal of Hydrology, 661, 133592. https://doi.org/10.1016/j.jhydrol.2025.133592.

[21] Fanyu Z., Jianbing P., Yong Z., Kezhou C., Qiuyang H. (2025). A homogenized sliding-block model for landslide motion analysis. Journal of Rock Mechanics and Geotechnical Engineering, 17, 7832-7847. https://doi.org/10.1016/j.jrmge.2025.02.019.

[22] Dumlu E., Güney M.Ş., Okan M. (2025). Numerical study of breaching at upper parts of homogenous earthen dams. Bull Eng Geol Environ 84, 22. https://doi.org/10.1007/s10064-024-04009-w

[23] Seric, I., Afkhami, S., Kondic, L. (2018). Direct numerical simulation of variable surface tension flows using a volume-of-fluid method. J Comput Phys, 352, 615–36. https://doi.org/10.1016/j.jcp.2017.10.008

[24] Issakhov, A., Zhandaulet, Y., Nogaeva A. (2018). Numerical simulation of dam break flow for various forms of the obstacle by VOF method. International Journal of Multiphase Flow, 109, 191-206. 10.1016/j.ijmultiphaseflow.2018.08.003

[25] Issakhov, A., Zhandaulet, Y. (2020). Numerical study of dam break waves on movable beds for complex terrain by volume of fluid method. Water Resources Management, 34, 463-480. DOI: 10.1007/s11269-019-02426-1

[26] Haltas, I., Tayfur, G., Elci, S. (2016). Two-dimensional numerical modeling of flood wave propagation in an urban area due to Urkmez dam-break, Izmir, Turkey. Nat Hazards, 81, 2103-2119. DOI: 10.1007/s11069-016-2175-6

[27] Oguz Simsek, Huseyin Islek, 2D and 3D numerical simulations of dam-break flow problem with RANS, DES, and LES, Ocean Engineering, Volume 276, 2023, 114298. https://doi.org/10.1016/j.oceaneng.2023.114298

[28] Saeid Esmaeeli Mohsenabadi, Ioan Nistor, Abdolmajid Mohammadian, and Hossein Kheirkhah Gildeh. 2023. CFD modelling of initial stages of dam-break flow. Canadian Journal of Civil Engineering. 50(10): 838-852. https://doi.org/10.1139/cjce-2021-0493

[29] Wen Qiu, Yanlong Li, Ye Zhang, Lifeng Wen, Ting Wang, Jing Wang, Xinjian Sun, Numerical investigation on the evolution process of cascade dam-break flood in the downstream earth-rock dam reservoir area based on coupled CFD-DEM, Journal of Hydrology, Volume 635, 2024, 131162. https://doi.org/10.1016/j.jhydrol.2024.131162

[30] Beteille, E., Larrarte, F., Boyaval, S., Demay, E., & Le, M. H. (2025). Dam-break flow over various obstacles configurations. Journal of Hydraulic Research, 63(2), 156–170. DOI:10.1080/00221686.2025.2460020

[31] Alibek I., Imanberdiyeva M., (2019). Numerical simulation of the movement of water surface of dam break flow by VOF methods for various obstacles. International Journal of Heat and Mass Transfer, 136, 1030-1051. https://doi.org/10.1016/j.ijheatmasstransfer.2019.03.034.

[32] Marsooli, R., Wu, W. (2014). 3-D finite-volume model of dam-break flow over uneven beds based on VOF method, Adv. Water Resour., 70, 104–117. DOI:10.1016/j.advwatres.2014.04.020

[33] Ozmen-Cagatay, H., Kocaman, S. (2011). Dam-break flow in the presence of obstacle: experiment and CFD simulation, Eng. Appl. Comp. Fluid, 5(4), 541– 552. DOI:10.1080/19942060.2011.11015393

[34] Xu, W. L., Chen, H. Y., Xue, Y., Niu, Z. P. (2013). The Chain of Dam Break in Cascade Reservoirs. China Water Power Press, 1, 12–24.